Nickel vacancy acceptor in nickel oxide: Doping beyond thermodynamic equilibrium

Robert Karsthof [*]

Felix Bloch Institute for Solid State Physics, Universitt Leipzig, Linnstrasse 5, 04103 Leipzig, Germany

Arthur Markus Anton [†]

Peter Debye Institute for Soft Matter Physics, Universitt Leipzig, Linnstrasse 5, 04103 Leipzig, Germany

Friedrich Kremer

Peter Debye Institute for Soft Matter Physics, Universität Leipzig, Linnéstrasse 5, 04103 Leipzig, Germany

Marius Grundmann [‡]

Felix Bloch Institute for Solid State Physics, Universität Leipzig, Linnéstrasse 5, 04103 Leipzig, Germany

(Received 20 January 2020; accepted 13 March 2020; published 30 March 2020)

This work reports on temperature-induced out-diffusion and concentration decay of the prominent intrinsic point defect V_{Ni} (nickel vacancy) in the wide-gap *p*-type semiconductor nickel oxide (NiO). V_{Ni} can easily be introduced into NiO thin films by offering high oxygen reactivity during film growth, rendering nonstoichiometric semiconducting material. However, exposure to lower oxygen reactivity after growth, e.g., in a standard atmosphere, usually leads to a gradual decrease of film conductivity, because the vacancy concentration returns to its thermodynamic equilibrium value. In this study we observe this process *in situ* by performing temperature-dependent measurements of the electrical conductivity on a room temperature-grown NiO film. At a temperature of 420 K under exclusion of oxygen, the doping level decreases by a factor of 8 while the associated room temperature DC conductivity drops by six orders of magnitude. At the same time, out-diffusion of the mobile V_{Ni} species can be indirectly observed through the occurrence of electrode polarization characteristics.

DOI: 10.1103/PhysRevMaterials.4.034601

I. INTRODUCTION

Nickel oxide (NiO) is a *p*-type wide-gap semiconducting oxide with promising properties for various device applications, a prominent one being a hole-transporting electrode in solar cells [1–4]. For these devices, NiO is typically doped intrinsically by an excess supply of reactive oxygen during film growth, which yields a large concentration of Ni vacancy defects (V_{Ni}) [5]. Because V_{Ni} is a double acceptor in NiO, this is the prominent method to obtain NiO thin films with semiconducting properties, apart from extrinsic doping with Li [5–7]. In a recent publication [8] we investigated the electronic transport properties of intrinsically doped NiO thin films and ascertain that polarons of intermediate size (about two lattice constants), strongly bound to acceptors, are the dominant charge carriers in these films. Electrical current is carried by hopping of these carriers exclusively among V_{Ni} sites without excitation to any extended states, i.e., band conduction is negligible. At temperatures above about half the Debye temperature θ_D ($\approx$200 K for NiO [9]) this is an over-the-barrier hopping process with an activation energy determined by the intersite separation. At temperatures lower than $\theta_D/2$ the activation energy is of the order of the width of the density of acceptor states. This implies that structural and electronic disorder play a central role in the temperature dependence of the electric conductivity of intrinsically doped NiO samples.

The degree of film nonstoichiometry is determined by the reactivity of the oxygen supply (i.e., ionized vs neutral) during film growth. High pressures and particle velocities develop at the laser ablation site on the target, leading to a high degree of ionization of the oxygen background gas. This favors a strong oxidation of the growing film. When exposed to ambient atmosphere, samples prepared in this way can be expected to be long-term unstable with regard to the Ni vacancy concentration. As a result, their conductivity is expected to decay with time, which is accelerated at elevated temperatures. This publication reports on the partially *in situ* experimental observation of this process. We believe the derived results are of importance for design rules of devices containing an intrinsically doped NiO layer, as in the case of hole-transport layers in solar cells for instance.

II. EXPERIMENTAL DETAILS

The NiO layers described here were fabricated by pulsed laser deposition (PLD), using a KrF excimer laser (wavelength

[*]Present address: Centre for Materials Science and Nanotechnology, Universitetet i Oslo, Gaustadalléen 23A, 0373 Oslo, Norway; r.m.karsthof@smn.uio.no

[†]Present address: Department of Physics and Astronomy, The University of Sheffield, Hicks Building, Hounsfield Road, Sheffield S3 7RH, United Kingdom.

[‡]Present address: Nano Team—Optical Microcavities, CRHEAC-NRS, rue Bernard Grgory, 06560 Valbonne, France.

 ©2020 American Physical Society

248nm, energy per pulse 650 mJ, repetition rate 10 Hz) from a ceramic NiO target (Alfa Aesar, purity 99.998%). During deposition, the O_2 partial pressure was kept at 0.1 mbar, and no intentional substrate heating was employed (room temperature growth). Two types of NiO thin film samples were fabricated. The first one consisted of NiO thin films deposited on a metallic Pt electrode on top of corundum substrates. These samples were used to study the electronic transport. The second type was NiO deposited on top of commercial fluorine-doped tin oxide (FTO)-covered glass substrates. Because of the high electron concentration in the FTO of 5×10^{20} cm^{-3}, this combination induces a space charge region in the NiO layer (pn^+ diode) which enabled the use of space charge spectroscopy to determine the doping level of the NiO. For both types, the NiO was capped by 20nm thick Pt layers. The deposition of NiO and Pt capping through a prior structured standard UV photoresist allowed their patterning by the lift-off technique into pillars with circular cross sections (diameters between 250 and 800 μm). All Pt layers were fabricated by DC magnetron sputtering. NiO film thicknesses were 260 nm for the undepleted (Pt/NiO/Pt) and 330 nm for the depleted (FTO/NiO/Pt) device structure.

Current-voltage characterization was done using a semi-automatic SÜSS wafer prober with tungsten needles and an AGILENT 4155C precision semiconductor parameter analyzer. The results of these measurements were used to select individual contacts for further characterization.

For capacitance-voltage measurements, the samples were mounted onto transistor sockets, and the selected contacts were wire bonded using Au wires and silver epoxy resin. For broadband dielectric spectroscopy (BDS) measurements, a similar method was applied, using a home-built sample holder instead of a transistor socket. The silver epoxy resin was hardened in a dry cabinet at 90 °C for 60 min.

BDS measurements were carried out in a temperature and frequency range between 300 and 420 K and between 10^{-2} and 10^{7} Hz, respectively, by means of a NOVOCONTROL Technology high-resolution α analyzer combined with a Quatro temperature controller (absolute thermal stability $\leqslant$1 K). Heating and cooling to a specific temperature was achieved in 6.6 min. The frequency sweeps at each temperature were done during 14.4 min, starting from high f. Overall, the average rate was 0.47 K min^{-1} during heating and 0.45 K min^{-1} during cooling.

X-ray diffraction was performed using a Philips X'Pert diffractometer and the Cu $K\alpha$ line ($\lambda = 1.5406$ Å).

III. RESULTS

The current density-voltage relations of the two structures shown in Fig. 1 demonstrate that the NiO layer on FTO exhibits a current rectification of approximately two orders of magnitude at ±2V, whereas the characteristics of the layer sandwiched between Pt electrodes show symmetric behavior with respect to voltage. The latter is therefore appropriate for the investigation of electrical transport, as previously done in Ref. [8]. It shall be noted that the transport is non-Ohmic, i.e., the differential conductivity increases with increasing voltage, as can be deducted from the linear plot of the j-V relation (inset of Fig. 1). The same behavior is observed in

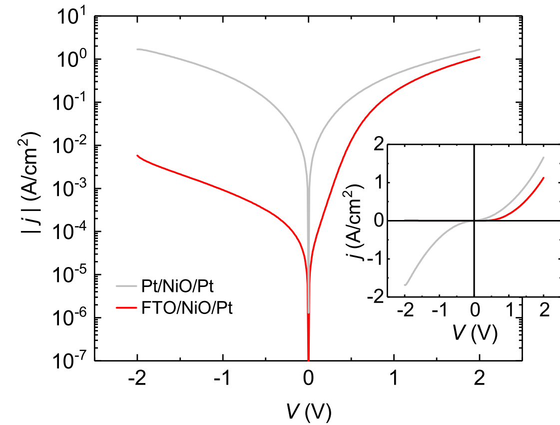

FIG. 1. Current density-voltage relations of selected Pt/NiO/Pt (symmetric behavior) and FTO/NiO/Pt (rectifying behavior) structures in semi-logarithmic and linear (inset) scale.

the forward region of the FTO/NiO diode (for voltage above ≈1 V). This behavior can be attributed to the specific DC transport mechanism of NiO which has similarities with space charge-limited conduction (SCLC) [10–12].

There are only a few reports of rectifying contacts comprising NiO as the carrier-depleted semiconductor. It has been shown that the low work function metals Al and Ti can be used to fabricate Schottky contacts on NiO [11], and the transparent conductive oxides tin-doped indium oxide (ITO) [12] and fluorine-doped tin oxide (FTO) [13] have been proven to be appropriate n-type partners for rectifying pn^+ heterostructures. A depletion region in a semiconductor enables the application of space charge spectroscopy techniques to investigate defect properties, such as the doping level and its spatial distribution. This is especially useful in the case of NiO because the determination of charge carrier concentration by Hall effect measurements is difficult due to extraordinarily low charge carrier mobility ($\mu_p \ll 0.1$ cm^2 V^{-1} s^{-1}).

In a recent publication [8] we reported on the electrical transport properties of NiO below room temperature. In the present work we address the same issue for elevated temperatures up to 420 K. Figure 2(a) shows the real part σ' of the complex conductivity $\sigma^* = \sigma' + i\sigma''$ of the Pt/NiO/Pt sample, recorded in a temperature cycle between 300 and 420 K. In general, the frequency dependence of σ' of the films can be separated into two different regions. At 300 K at the beginning of the cycle, σ' is independent of the frequency of the electric field f up to 10^3 Hz. This is interpreted here as the DC conductivity limit of the electronic conduction process σ_{dc}. With increasing f, σ' begins to exhibit dispersion, rising slowly in the form of a broadened step.

The complex dielectric function ε^* and the complex conductivity σ^* are connected by the relation

$$\varepsilon^* = \frac{1}{2\pi i f \varepsilon_0}\sigma^*, \qquad (1)$$

The transformation of our measured σ' data into ε'' representation is shown in Fig. 2(b) for selected temperatures. If slow processes, for example relaxation of molecular dipoles or polarization processes, which are unable to follow above a certain cutoff frequency of the AC field, occur within

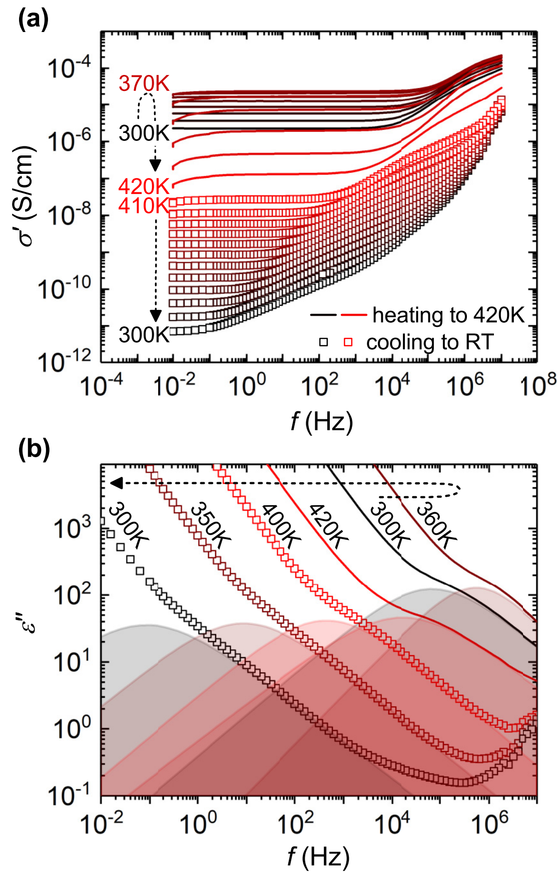

FIG. 2. (a) Real part σ' of the complex conductivity function $\sigma^* = \sigma' + i\sigma''$ of a Pt/NiO/Pt structure, measured by BDS in a temperature cycle between room temperature and 420 K. (b) Dielectric loss representation of the same data set for selected temperatures, including fits to the MWS polarization according to (3) (shaded areas).

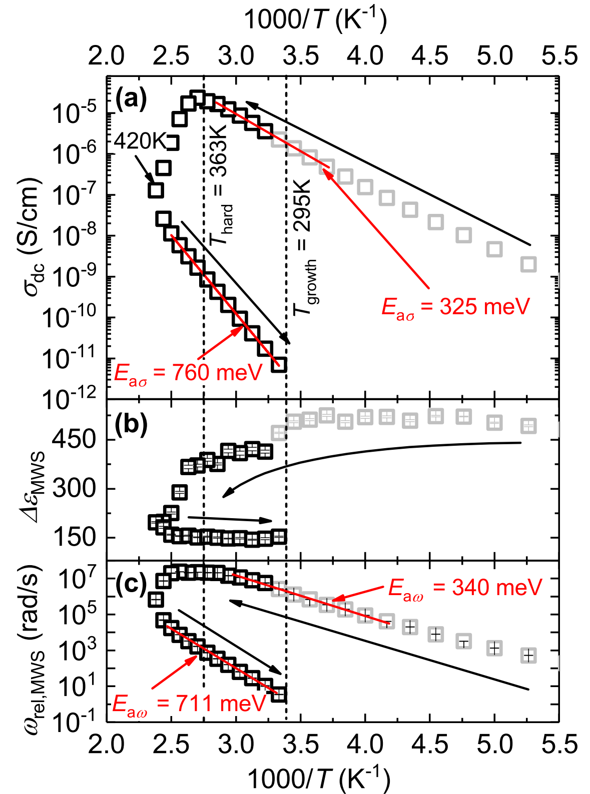

FIG. 3. (a) DC conductivity, (b) relaxation strength, and (c) rate of the MWS polarization mode for temperatures above 300 K (black symbols), obtained from fits of $\varepsilon''(\omega)$ according to (3). Representative data points from measurements below 300 K are shown in addition (gray symbols) [8]. Red lines: Arrhenius-type fits used to extract the shown activation energies. Growth and epoxy hardening temperatures indicated by vertical dashed lines.

the investigated frequency window, these become visible as peaks (or in the present case shoulders) in the imaginary part of ε^*, $\varepsilon'' = \frac{1}{\omega\varepsilon_0}\sigma'$. In the present case, one such process can be recognized in the data of Fig. 2(b). In our recent paper [8] we showed that this is the signature of a dielectric polarization process connected to the spatial inhomogeneity of σ^* (Maxwell-Wagner-Sillars (MWS) polarization [14]) which is caused by the large degree of disorder present in room temperature-deposited NiO. More precisely, the RT-grown NiO layer consists of conductive grains embedded into a matrix of semi-insulating grain boundaries. Under AC electric fields, such an arrangement exhibits charge carrier polarization within the grains on a length scale of the order of the grain diameter. Features in ε^* related to relaxation processes can generally be fitted with a Debye-type function or modifications thereof; in the present case, we used the Cole-Cole relation [15]

$$\varepsilon^* = \varepsilon_\infty + \frac{\varepsilon_s - \varepsilon_\infty}{1 + (i\omega\tau_{rel})^{1-b}}, \quad (2)$$

with ε_∞ and ε_s the high-frequency and static value of the relative dielectric permittivity, $\omega = 2\pi f$, τ_{rel} is the relaxation time constant, and $b \in [0, 1)$ is a dimensionless broadening parameter, respectively. Taking additional account of the DC conductivity, the following relation [15] was used to fit the ε'' data:

$$\varepsilon''(\omega) = \frac{\sigma_{dc}}{\omega\varepsilon_0} + \frac{\Delta\varepsilon}{2}\frac{\cos b\pi/2}{\cosh[(1-b)\ln(\omega\tau_{rel})] + \sin b\pi/2}, \quad (3)$$

where σ_{dc} is the DC conductivity taken as the value of σ' at the low-frequency plateau and $\Delta\varepsilon = \varepsilon_s - \varepsilon_\infty$. The imaginary part of the dielectric function ε'', and the fits to the MWS polarization process according to (3) (without the DC contribution), are also shown in Fig. 2(b) as shaded areas. The temperature dependence of σ_{dc}, $\Delta\varepsilon_{MWS}$, and $\omega_{rel,MWS}$ obtained by the fits are displayed in Fig. 3. Figure S3 of the Supplemental Material [16] shows the analogously modeled real part ε' of ε^* based on the same values of fitting parameters, demonstrating the high quality of the fits.

A simplifying model of polarization processes due to a spatially varying dielectric function, like in the case of MWS polarization, considers spherical filler particles (represented in this experiment by the grain interior, volume fraction φ_f) with conductivity σ'_f embedded in a matrix with lower conductivity $\sigma'_m \ll \sigma'_f$ (here grain boundaries), reflecting the nature of the NiO film described earlier. Both media are assumed to have the same real part of the dielectric function ε'. It can be shown [14] that in this case a Debye-like relaxation peak,

representing Maxwell-Wagner-Sillars polarization, occurs, with

$$\Delta\varepsilon_{\rm MWS} \approx 3\varepsilon' \left(\frac{\sigma'_{\rm f}}{\sigma'_{\rm m}}\right)^2 \frac{\varphi_{\rm f}(1-\varphi_{\rm f})}{(2+\varphi_{\rm f})^2} \quad (4)$$

and

$$\tau_{\rm rel,MWS} \approx 3\varepsilon_0\varepsilon' \frac{1}{(1-\varphi_{\rm f})\sigma'_{\rm f}}. \quad (5)$$

Therefore, depending on the "conductivity contrast" between filler and matrix, $\Delta\varepsilon$ can attain larger values than commonly considered for molecular relaxation processes (typically $\Delta\varepsilon \ll 1$). Moreover, (5) demonstrates that the relaxation rate $\omega_{\rm rel,MWS} = 2\pi\tau^{-1}_{\rm rel,MWS}$ is directly proportional to the conductivity of the filler, implying that it roughly exhibits the same activation energy.

Because the film was grown at room temperature and the measurement is done at elevated temperatures, the presented experiment can be considered an *in situ* annealing experiment conducted under oxygen-poor conditions (pure N_2 atmosphere). At temperatures above about 360 K three annealing-induced features appear simultaneously: (i) The frequency-independent contribution $\sigma_{\rm dc}$ drops, even though the temperature is increased to 420 K. During subsequent cooling to room temperature, $\sigma_{\rm dc}$ decreases further, as expected due to the decreasing temperature, resulting in a final reduction of six orders of magnitude as compared to the initial (room temperature) value (see Fig. 3, top panel). (ii) Electrode polarization sets in, causing a drop of σ' at very low frequencies [Fig. 2(a)]. (iii) The MWS polarization process strongly decreases in both relaxation strength $\Delta\varepsilon_{\rm MWS}$ and relaxation rate $\omega_{\rm rel,MWS}$ [Figs. 3(b) and 3(c)]. Note that 363 K is the temperature at which the sample was kept to harden the conductive epoxy after wire bonding, and justifiably marks the onset of an accelerated thermal change of the already partially treated film. Furthermore, a sudden drop of the dielectric strength of the MWS polarization $\Delta\varepsilon_{\rm MWS}$ can already be seen above room temperature, at which the NiO film had been deposited.

We attribute observations (i) to (iii) to the thermally induced out-diffusion of Ni vacancies. Because the initial concentration of $V_{\rm Ni}$ is much higher than the thermodynamically adequate level, the film has the tendency to equilibrate this concentration at any given temperature, especially at $T > T_{\rm growth}$. This is achieved by the diffusion of $V_{\rm Ni}$ to the sample surface where they decay by locally dissolving the crystal [17] according to the reaction

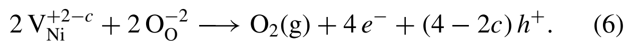

$$2\,V_{\rm Ni}^{+2-c} + 2\,O_{\rm O}^{-2} \longrightarrow O_2({\rm g}) + 4\,e^- + (4-2c)\,h^+. \quad (6)$$

This renders the film interior less conductive. Equation (6) also includes the formal charges that are attributed to the constituents. Ideally, each O site carries a formal -2 charge while that of each $V_{\rm Ni}$ acceptor is $+2$. Due to the presence of compensating donor states ("hole killers"), however, a fraction $0 < c < 1$ of the vacancies is ionized. The reaction therefore produces a net charge of $-2c \cdot e$ per destroyed vacancy site. Since the sample surface consists mostly of the film/electrode interface (film thickness $\ll$ contact diameter), these charges temporarily accumulate in its vicinity and thereby partially screen the interior of the sample from the applied AC electric field, before they migrate into the electrode. This leads to an apparently lower electric conductivity of the sample, an effect termed electrode polarization (EP) [14,18,19]. Because this effect is in principle comparable to ionic conduction, the role of transported ions played by the diffusing partially charged $V_{\rm Ni}$ defects in the present case, the characteristic frequency of an EP process is determined by the ion diffusivity and is therefore typically low; here EP can be seen to dominate σ' below 1 Hz [Fig. 2(a)].

On the basis of the conductivity model developed in our recent work [8], a decrease of the acceptor density is expected to be accompanied by an increase of the activation energy of $\sigma_{\rm dc}$. This is the direct result of the increased interacceptor distance, due to the $V_{\rm Ni}$ decay, and is observed here, as Fig. 3(a) demonstrates: $E_{\rm a,\sigma}$ increases from 325 before to 760 meV after the high-temperature BDS measurement. The decrease of $\Delta\varepsilon_{\rm MWS}$ and $\omega_{\rm rel,MWS}$ of the MWS polarization process as a consequence of annealing [Figs. 3(b) and 3(c)] is also in accordance with the model, because both parameters are affected by the conductivity of the film [Eqs. (4) and (5)]. In particular, $\omega_{\rm rel,MWS}$ exhibits almost the same activation energy (340 before and 711 meV after annealing) as $\sigma_{\rm dc}$.

C-V measurements are a well-established method to determine the density of dopants and traps in a semiconductor. In order to perform the measurement, a rectifying contact inducing a space charge (or depletion) region in the semiconductor is necessary, usually a metal-semiconductor or one-sided *pn* junction. During a slow voltage sweep to increasingly negative V, the capacitance C of the depletion layer in the semiconductor under study is measured dynamically, i.e., with an additional (small) AC voltage signal. Applying a reverse bias increases the width w of the space charge region; therefore the probing point is shifted into the semiconductor, and a doping profile can be constructed by using the relations [20]

$$N_{\rm net} = \frac{2}{e\varepsilon_{\rm s}\varepsilon_0 A^2}\left(\frac{d}{dV}C^{-2}\right)^{-1},$$
$$w = \frac{\varepsilon_{\rm s}\varepsilon_0 A}{C}. \quad (7)$$

In order to relate the decrease of conductivity to a lower $V_{\rm Ni}$ density, the NiO doping density was determined on the FTO/NiO sample. Due to the occurrence of charge depletion almost exclusively in the NiO layer (one-sided pn^+ diode), *C-V* measurements could be conducted on this sample. It was subjected to a thermal treatment at 420 K in N_2 atmosphere for 2 h to mimic the conditions during the high-temperature BDS measurement.

The measurement frequency during *C-V* has to be adjusted to a value as low as possible to record contributions also from deep-lying defects, but keeping signal-to-noise ratio as high as possible. In this case, 5 kHz was chosen. The averaged net doping obtained by this method decreases from initially 4.4×10^{18} to $6.2 \times 10^{17} {\rm cm}^{-3}$, as is shown in Fig. 4. Because the doping level is mainly determined by the dominant acceptor $V_{\rm Ni}$ [5], this result confirms the out-diffusion of the $V_{\rm Ni}$ acceptors and corroborates the distinct decrease of the film conductivity. Note that also in the case of the annealed NiO, the width of the depletion region ($\leqslant$130 nm) is still lower than

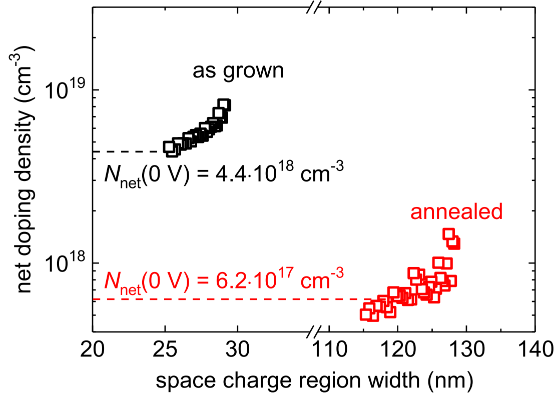

FIG. 4. Doping profiles of a selected NiO/FTO contact before and after annealing at 420 °C in N_2. The measurement frequency was 5 kHz. Doping levels measured under $V = 0$ V indicated by horizontal lines.

the total NiO film thickness (330 nm), which is important for the measured doping level to be reliable.

X-ray diffraction (XRD) measurements were carried out on a Pt/NiO reference sample before and after an annealing step (420 K in N_2 atmosphere for 2 h). The position and broadening of the NiO (111) reflex remains unchanged by this procedure (see Fig. S1, Supplemental Material [16]), which suggests that a temperature of 420 K does not induce significant structural changes to room temperature-grown NiO films. Therefore, we conclude that the observed annealing-induced changes of electrical transport properties are entirely due to the removal of V_{Ni} defects.

The observed processes are summarized in Fig. 5 and as follows. The growth of NiO films by PLD takes place under conditions strongly deviating from thermodynamic equilibrium. This leads to a concentration of defects in the growing film that is considerably higher than in thermodynamic equilibrium, which holds in particular true for V_{Ni} as it is the dominant intrinsic point defect [Fig. 5(a)]. Charge transport is facilitated through hopping conduction over initially low barriers between neighboring vacancy sites [Fig. 5(c)]. On the other hand, the structural inhomogeneity gives rise to the MWS polarization of conductive grains embedded in a semi-insulating matrix (grain boundaries) which produces the according spectral relaxation process shown in Fig. 5(b).

At elevated temperatures, the V_{Ni} defects become mobile. They diffuse though the film, likely via consecutive transferrals of Ni ions into the vacancy sites. The activation energy for this migration has been determined by several authors [21,22] to be in the range of 1.92 to 2.56 eV. A large fraction of diffusing vacancies reaches the film/electrode interfaces, where they dissolve as described by (6). At room temperature, the diffusion is not efficient, leading to a rather slow decay of the vacancy concentration. Because the films have been kept at room temperature before the BDS measurement for several days, however, some equilibration may already have taken place. Increasing the temperature to above 300 K significantly enhances the decay rate: $\omega_{rel,MWS}$ rises slower than below room temperature (see also Fig. S2, Supplemental Material [16]). In addition, $\Delta\varepsilon_{MWS}$ clearly drops from ≈520 to ≈350 between 300 and 360 K. However, the most pronounced acceleration of the V_{Ni} decay process can be seen above 360 K, because this was the temperature at which the sample

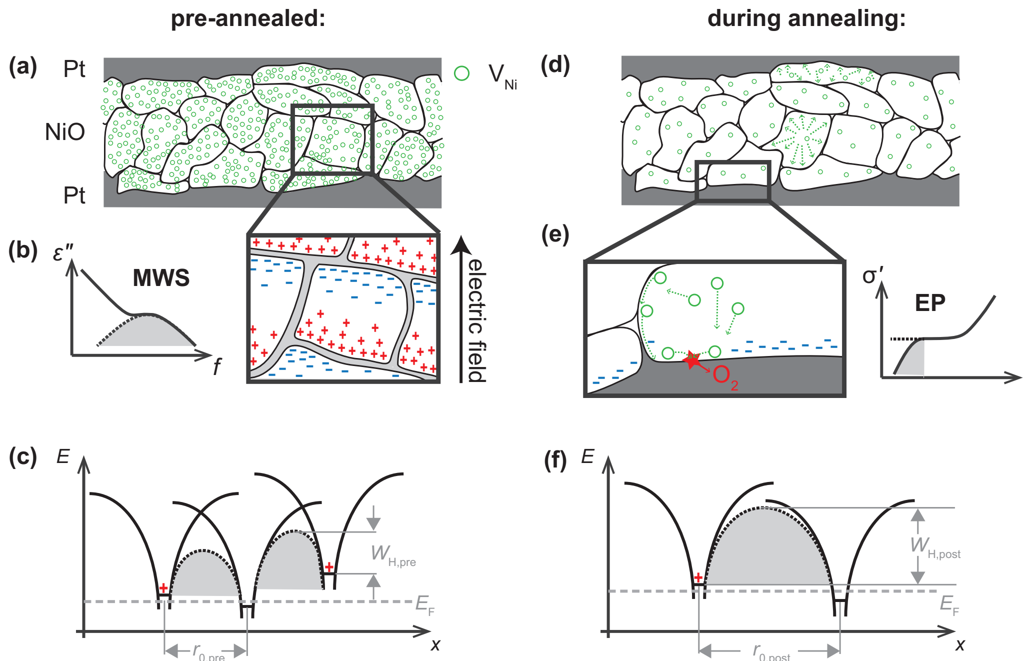

FIG. 5. Annealing-induced effects of V_{Ni} out-diffusion. (a) Schematic cross-sectional view of the film before annealing with high density of V_{Ni}, (b) polarization of mobile charges within grains under AC electric field leads to dielectric loss peak (Maxwell-Wagner-Sillars polarization, MWS), and (c) interacceptor barriers for hopping transport $W_{H,pre}$ are low. (d) During annealing, the V_{Ni} concentration decreases due to out-diffusion to the film/electrode interface, where (e) oxygen is released from the film, leaving behind uncompensated negative charges that lead to electrode polarization (EP). (f) Lower V_{Ni} concentration results in enhanced hopping barriers $W_{H,post}$ between adjacent acceptors.

was kept during hardening the silver epoxy. Furthermore, as soon as the temperature is lowered again, the diffusion of V_{Ni} slows down dramatically. When the sample is exposed to a second temperature cycle (see Fig. S4, Supplemental Material [16]), the out-diffusion again increases above 300 K, however, to a much lesser extent than during the first run.

This out-diffusion process is important to monitor when designing devices that are based on semiconducting, Ni-deficient NiO. In many technologically relevant cases, reactively sputtered NiO films are employed, where the deviation from stoichiometry is even more pronounced. When such films are used in devices where operation leads to heating, the device performance can be critically impaired by the decay of the V_{Ni} acceptor.

IV. CONCLUSION

Room temperature-grown NiO thin films were investigated by broad-band dielectric spectroscopy (BDS) measurements between 300 and 420 K, allowing an *in situ* observation of annealing-induced effects on the frequency- and temperature-dependent conductivity σ'. It was shown that out-diffusion of the dominant intrinsic acceptor V_{Ni} (Ni vacancy) leads to a lower net doping level of the film (about a factor of 8), as determined by capacitance-voltage profiling. This, in turn, decreases the film conductivity at room temperatures by six orders of magnitude. The existence of mobile ionic species to which the charges are bound is supported by the observation of electrode polarization effects that accompany the drop of σ_{dc}. Simultaneously, strength and relaxation rate of a polarization process, which dominates the dispersion of the dielectric function, are strongly reduced. This is in accordance with our previous assignment of this relaxation process as a phenomenon induced by spatially varying σ', also known as Maxwell-Wagner-Sillars polarization.

ACKNOWLEDGMENTS

This work was funded by the Deutsche Forschungsgemeinschaft (DFG, German Research Foundation) project number 31047526, SFB762, project B06, and "SFB/TRR 102: Polymers under Multiple Constraints" (Project No. B08). In addition, Arthur Markus Anton is thankful financial support from the DFG project AN 1523/1-1. We thank M. E. Bathen and K. H. Nygård for help with revising the manuscript.

There are no conflicts to declare.

[1] J. He, H. Lindström, A. Hagfeldt, and S.-E. Lindquist, Dye-sensitized nanostructured p-type nickel oxide film as a photocathode for a solar cell, J. Phys. Chem. B **103**, 8940 (1999).

[2] M. D. Irwin, D. B. Buchholz, A. W. Hains, R. P. H. Chang, and T. J. Marks, *p*-type semiconducting nickel oxide as an efficiency-enhancing anode interfacial layer in polymer bulk-heterojunction solar cells, Proc. Natl. Acad. Sci. USA **105**, 2783 (2008).

[3] S.-Y. Park, H.-R. Kim, Y.-J. Kang, D.-H. Kim, and J.-W. Kang, Organic solar cells employing magnetron sputtered p-type nickel oxide thin film as the anode buffer layer, Sol. Energy Mater. Sol. Cells **94**, 2332 (2010).

[4] J.-Y. Jeng, K.-C. Chen, T.-Y. Chiang, P.-Y. Lin, T.-D. Tsai, Y.-C. Chang, T.-F. Guo, P. Chen, T.-C. Wen, and Y.-J. Hsu, Nickel oxide electrode interlayer in $CH_3NH_3PbI_3$ perovskite/PCBM planar-heterojunction hybrid solar cells, Adv. Mater. **26**, 4107 (2014).

[5] S. Lany, J. Osorio-Guillén, and A. Zunger, Origins of the doping asymmetry in oxides: Hole doping in NiO versus electron doping in ZnO, Phys. Rev. B **75**, 241203 (2007).

[6] U. Joshi, Y. Matsumoto, K. Itaka, M. Sumiya, and H. Koinuma, Combinatorial synthesis of Li-doped NiO thin films and their transparent conducting properties, Appl. Surf. Sci. **252**, 2524 (2006).

[7] T. Dutta, P. Gupta, A. Gupta, and J. Narayan, Effect of Li doping in NiO thin films on its transparent and conducting properties and its application in heteroepitaxial p-n junctions, J. Appl. Phys. **108**, 083715 (2010).

[8] R. Karsthof, M. Grundmann, A. M. Anton, and F. Kremer, Polaronic interacceptor hopping transport in intrinsically doped nickel oxide, Phys. Rev. B **99**, 235201 (2019).

[9] R. G. Allen, T. E. Stephenson, C. P. Stanford, and S. Bernstein, Slow neutron cross sections of gold, silver, indium, nickel, and nickel oxide, Phys. Rev. **96**, 1297 (1954).

[10] A. Rose, Space-charge-limited currents in solids, Phys. Rev. **97**, 1538 (1955).

[11] S. Seo, M. J. Lee, D. C. Kim, S. E. Ahn, B.-H. Park, Y. S. Kim, I. K. Yoo, I. S. Byun, I. R. Hwang, S. H. Kim *et al.*, Electrode dependence of resistance switching in polycrystalline NiO films, Appl. Phys. Lett. **87**, 263507 (2005).

[12] H.-L. Chang, T. C. Lu, H. C. Kuo, and S. C. Wang, Effect of oxygen on characteristics of nickel oxide/indium tin oxide heterojunction diodes, J. Appl. Phys. **100**, 124503 (2006).

[13] E. Thimsen, A. B. F. Martinson, J. W. Elam, and M. J. Pellin, Energy levels, electronic properties, and rectification in ultrathin p-NiO films synthesized by atomic layer deposition, J. Phys. Chem. C **116**, 16830 (2012).

[14] F. Kremer and A. Schönhals, *Broadband Dielectric Spectroscopy* (Springer, Berlin, 2002).

[15] K. S. Cole and R. H. Cole, Dispersion and absorption in dielectrics. I. Alternating current characteristics, J. Chem. Phys. **9**, 341 (1941).

[16] See Supplemental Material at http://link.aps.org/supplemental/10.1103/PhysRevMaterials.4.034601 for data on structural changes induced by annealing, temperature dependence of the difference quotient of $\omega_{rel,MWS}$, quality of fits to MWS polarization process with respect to ε' data, and BDS data for a second high-temperature cycle.

[17] There are experiments that have directly detected the reversion of this process (e.g., the creation of Ni vacancies at elevated temperatures through the equilibration in O_2 gas) by thermogravimetric methods, for example by Mitoff [23], and Osburn and Vest [24].

[18] A. Serghei, M. Tress, J. R. Sangoro, and F. Kremer, Electrode polarization and charge transport at solid interfaces, Phys. Rev. B **80**, 184301 (2009).

[19] P. B. Ishai, M. S. Talary, A. Caduff, E. Levy, and Y. Feldman, Electrode polarization in dielectric measurements: A review, Meas. Sci. Technol. **24**, 102001 (2013).

[20] C. van Opdorp, Capacitance—voltage relations of Schottky and p-n diodes in the presence of both shallow and deep impurities, Phys. Status Solidi B **32**, 81 (1969).

[21] M. T. Shim and W. J. Moore, Diffusion of nickel in nickel oxide, J. Chem. Phys. **26**, 802 (1957).

[22] A. Atkinson and R. I. Taylor, The diffusion of Ni in the bulk and along dislocations in NiO single crystals, Philos. Mag. A **39**, 581 (1979).

[23] S. P. Mitoff, Electrical conductivity and thermodynamic equilibrium in nickel oxide, J. Chem. Phys. **35**, 882 (1961).

[24] C. Osburn and R. Vest, Defect structure and electrical properties of NiO—I. high temperature, J. Phys. Chem. Solids **32**, 1331 (1971).